

AN ABSTRACT OF THE THESIS OF

MARK ERIE ODEGARD for the Master of Science in Physics
(Name) (Degree) (Major)

Date thesis is presented May 12, 1965

Title GRAVITY INTERPRETATION USING THE FOURIER INTEGRAL

Abstract approved 

The gravitational anomalies of simple bodies (sphere, cylinder, and fault) were used to develop methods for analyzing gravity data in the frequency domain. The Fourier transforms of the functional representations of the theoretical gravitational anomalies of these bodies were obtained. Mathematical formulations were made between the transform versus frequency relationships and the depths and sizes of the bodies. Compound gravity anomalies (multiple cylinders, fault and cylinder) were analyzed, and the transforms were reduced to transforms of anomalies due to individual simple bodies. The methods of analyses were applied to theoretical anomalies using numerical techniques, and the accuracy of both depth and size determinations was within a few percent in all cases.

GRAVITY INTERPRETATION USING THE FOURIER INTEGRAL

by

MARK ERIE ODEGARD

A THESIS

submitted to

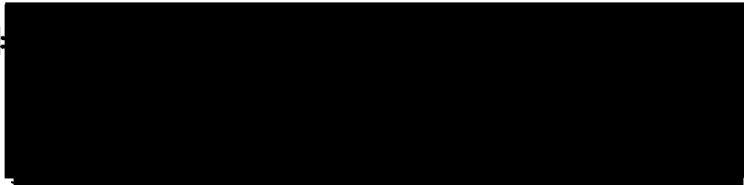
OREGON STATE UNIVERSITY

in partial fulfillment of
the requirements for the
degree of

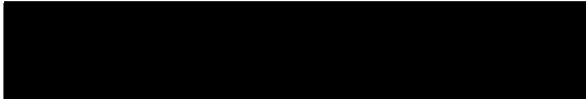
MASTER OF SCIENCE

June 1965

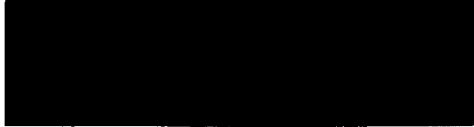
APPROVED:

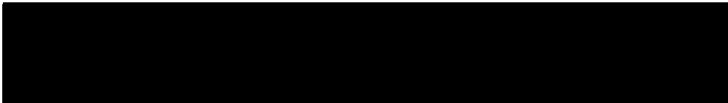

Professor of Oceanography


In Charge of Major


Associate Professor of Physics

In Charge of Major


Head of Department of Physics


Head of Department of Oceanography


Dean of Graduate School

Date thesis is presented May 13, 1965

Typed by Patricia C. Hazeltine

ACKNOWLEDGMENTS

The work presented in this thesis was performed under the direction of Dr. Joseph W. Berg, Jr. The writer wishes to thank Dr. Berg for his guidance in all phases of the research and preparation of the manuscript.

Appreciation is extended to Dr. Harold R. Vinyard for his assistance in the preparation of the thesis.

The computer programs used in this research were prepared with the help of Mrs. Susan J. Borden.

This research was sponsored by the American Petroleum Institute, API Grant-in-aid 141, and by the National Science Foundation, grant NSF-G24353 and GP2808.

TABLE OF CONTENTS

	Page
Introduction	1
Method of Analysis	4
I. Transforms and analysis of simple bodies	4
(a) Cylinder	4
(b) Sphere	6
(c) Fault	16
II. Transforms and analysis of more complex structures	21
(a) Multiple cylinders	21
(b) Cylinder and fault	23
III. Results and accuracy of analysis	25
Summary and Conclusions	29
Bibliography	30
Appendix A	31
Some properties of the Fourier Integral	31
Displacement theorem	32
Appendix B	33
Integration of the sphere and fault transforms	33
(a) Sphere	33
(b) Fault	34
Appendix C	37
Description of the transform program	37

LIST OF FIGURES

<u>Fig.</u>		<u>Page</u>
1a.	Vertical gravity, $g_z(X)$, over infinite horizontal cylinder vs distance, X	5
1b.	Fourier transform of vertical gravity of infinite horizontal cylinder, $F_c(\omega)$, vs frequency, ω	5
2a.	Vertical gravity, $g_z(X)$, over sphere vs distance, X	7
2b.	Fourier transform of vertical gravity of sphere, $F_s(\omega)$, vs frequency, ω	7
3.	Maximum frequency used in approximation vs depth of burial, D	10
4a.	Approximation constant, A_1 , vs depth, D , for depths less than 2 km.	11
4b.	Approximation constant, A_2 , vs depth, D , for depths less than 2 km.	12
4c.	Approximation constant, A_1 , vs depth, D , for depths greater than 1 km.	13
4d.	Approximation constant, A_2 , vs depth, D , for depths greater than 1 km.	14
5.	Ratios of approximate intercept, $F_{SA}(0)$, to actual intercept, $F_s(0)$, of Fourier transform of vertical gravity of sphere.	15
6a.	Vertical gravity over fault, $g_z(X)$, vs distance, X	17
6b.	Fourier transform, $F_f(\omega)$, of vertical gravity over fault vs frequency, ω	17
6c.	Modified Fourier transform, $f(\omega)$, $\left[f(\omega) = \omega F_f(\omega) \right]$ vs frequency to determine $\sqrt{2\pi} \lambda \sigma T$	19
6d.	Reduced Fourier transform, $G(\omega)$, vs frequency, ω , used to determine depth and throw of fault.	20
7a.	Calculated vertical gravity over two infinite horizontal cylinders vs distance, X	22

<u>Fig.</u>		<u>Page</u>
7b.	Fourier transform, $F(\omega)$, of calculated vertical gravity over two infinite horizontal cylinders vs frequency, ..	22
8a.	Calculated vertical gravity over fault and cylinder offset from fault by distance, Y	24
8b.	Fourier transform of cylinder extracted from total calculated Fourier transform by considering only real parts of the total calculated transform.	26
8c.	Fourier transform of fault extracted from total calculated Fourier transform by the real part (transform of cylinder) from the total calculated transform.. . . .	27
9.	Magnification of error by subtraction of successive half cycles.	38

LIST OF TABLES

<u>Table</u>	<u>Page</u>
I. Computed and actual data for multiple cylinders.	28
II. Computed and actual data for cylinder and fault.	28

GRAVITY INTERPRETATION USING THE FOURIER INTEGRAL

INTRODUCTION

For more than a hundred years the Fourier Integral has been used as a method of analysis. One of the earliest examples is the experiment by Fizeau (1862), in which he demonstrated that the sodium-D line was a doublet long before it had been observed directly. Other examples of its use are provided in nearly every area of science.

Although the Fourier Integral method has usually been applied to data which exhibit wave characteristics, any function satisfying certain conditions (see Appendix A) can be transformed into a complementary function by use of the Fourier Transform. This complementary function contains all information about the event or data described by the original function. So the Fourier Integral has been used in the analysis of data not directly related to frequency defined phenomena. In particular it has been recognized that the earth acts as a low-pass filter with respect to gravitational and magnetic anomalies which originate at depth in the earth (Dean, 1958). These phenomena can be described by utilization of the Fourier Integral.

Dean (1958) and Goldstein and Ward (Personal Communication) used Fourier analysis to determine the effects of filtering gravitational data. Other investigators (among which are Tsuboi and Fuchida (1938) and Tomoda and Aki (1955)) have used the Fourier Integral in the downward continuation of the gravitational field to describe sub-surface density distributions. The research presented in this thesis differs from the previous work in that the primary emphasis is on the analysis of the frequency spectrum to determine information about

the depths, sizes, and densities of disturbing bodies buried at depth.¹

The object of this research was to determine the feasibility of using the Fourier Integral for the direct analysis of gravitational data. It has been pointed out by many authors that it is theoretically impossible to determine a unique density distribution beneath the surface of the earth from the potential field measured at the surface. However, if assumptions are made about the nature of the density distribution, a unique solution can be determined (Peters, 1949). In this research the density distributions were assumed to be in the shapes of regular bodies (cylinder, sphere, and fault). Integrations of the functional representations of the theoretical gravitational anomalies of these bodies were performed to obtain their Fourier Transforms. Exact integrals were obtained for each of the bodies used in the research. The Fourier Transforms were investigated to determine possible relationships between slopes and intercepts of the amplitude versus frequency data and the depths, sizes, and density contrasts of the bodies. Methods were devised to determine these parameters from the transforms.

Transforms of the anomalies of more complex structures composed of simple bodies were investigated to determine whether the method

¹After this research was completed, an article by Solov'yev (1962) was obtained and translated. Research of a nature similar to the research in this thesis was presented by Solov'yev. However, his analyses were performed using magnetic anomalies caused by dikes.

could resolve these complex structures into their simpler components. These cases were tested by doing numerical integrations of the digitized theoretical anomalies. At this time, techniques for handling the data were established.

METHOD OF ANALYSIS

I. Transforms and Analysis of Simple Bodies

In this section the functional representations of the transforms of the gravitational anomalies due to simple bodies are presented, and the methods are described by which the data were analyzed to determine the parameters that describe the bodies. The method of analysis for the (a) cylinder, (b) sphere, and (c) fault will be discussed in the order given.

(a) Cylinder

The vertical gravity at each point along a profile perpendicular to a buried cylinder² (Figure 1a) is given by

$$g_z(X) = \beta D / (D^2 + X^2) \quad (1)$$

where

$$\beta = 2\pi \gamma R_c^2 \sigma$$

γ = universal gravitational constant

R_c = radius of cylinder

σ = density contrast

D = depth to center of cylinder

X = horizontal surface distance

²The formulas for the gravity field of the cylinder, sphere, and fault were taken from Nettleton (1940).

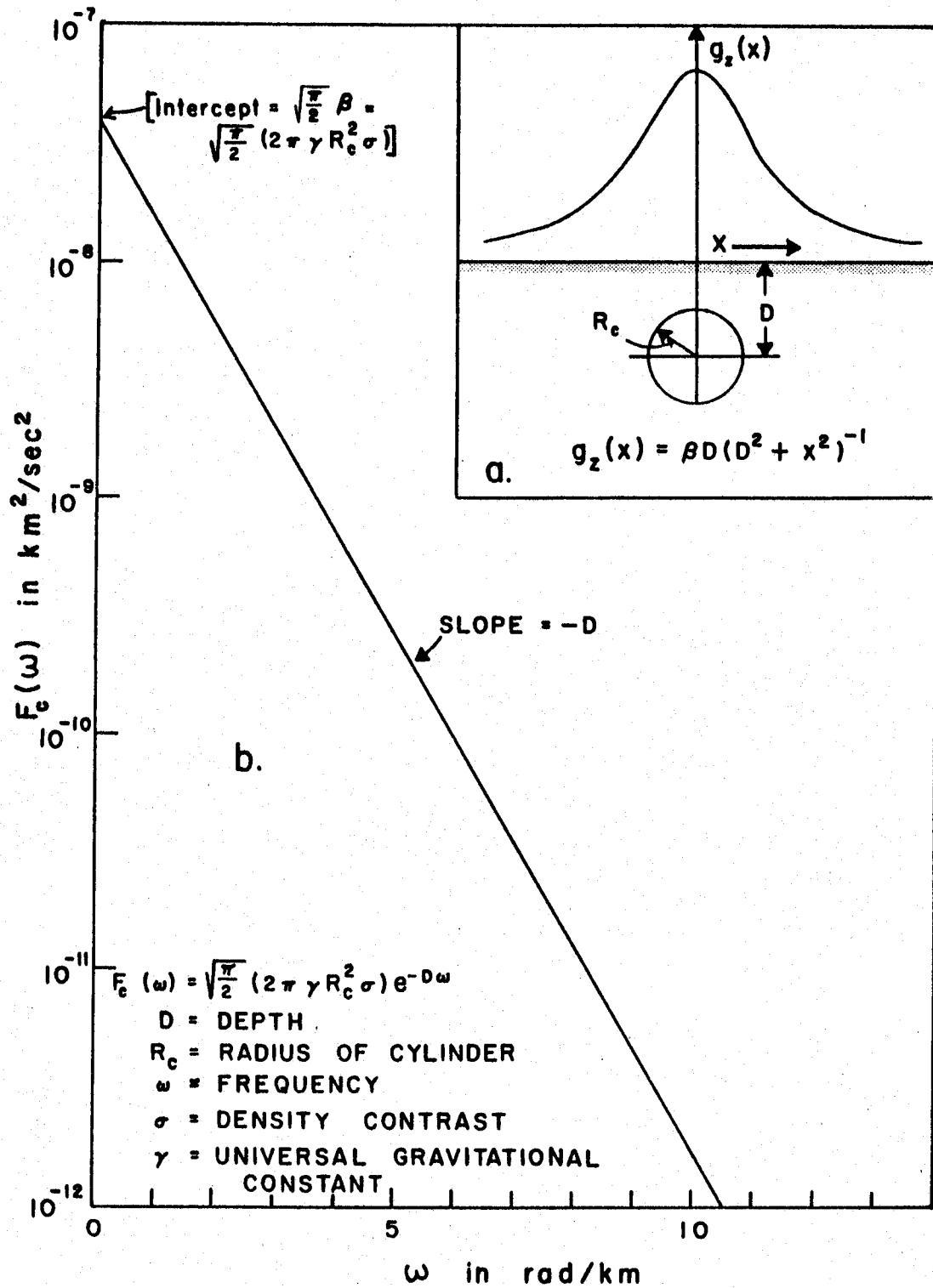


Figure 1a. Vertical gravity, $g_z(X)$, over infinite horizontal cylinder vs distance, X .

Figure 1b. Fourier transform of vertical gravity of infinite horizontal cylinder, $F_c(\omega)$, vs frequency, ω .

The vertical gravity for a cylinder is an even function $[f(x) = f(-x)]$, so the Fourier Transform is given by (see Appendix A)

$$F_c(\omega) = \frac{2\beta D}{\sqrt{2\pi}} \int_0^{\infty} (D^2 + \phi^2)^{-1} \cos(\omega \phi) d\phi \quad (2)$$

The integration tables (Dewight, 1961) give for this integral

$$F_c(\omega) = \sqrt{\frac{\pi}{2}} \beta e^{-D\omega} \quad (3)$$

Where ω is the frequency in cycles per unit length.

A plot of the exact integral, $F_c(\omega)$, against frequency, ω , on a semilogarithmic scale is shown in Figure 1b. This relationship

$$\ln[F_c(\omega)] = \ln\left(\sqrt{\frac{\pi}{2}} \beta\right) - D\omega \quad (4)$$

is linear with the slope equal to the negative of the depth. The intercept

$$I = \sqrt{\frac{\pi}{2}} \beta = \sqrt{\frac{\pi}{2}} 2\pi \gamma R_c^2 \sigma \quad (5)$$

gives the relative size of the cylinder

$$R_c^2 \sigma = \frac{I}{2\pi \gamma} \sqrt{\frac{2}{\pi}} \quad (6)$$

(b) Sphere

The vertical gravity at each point along a profile which passes over the center of a buried sphere (Figure 2a) is given by

$$g_z(X) = \alpha D / (D^2 + X^2)^{3/2} \quad (7)$$

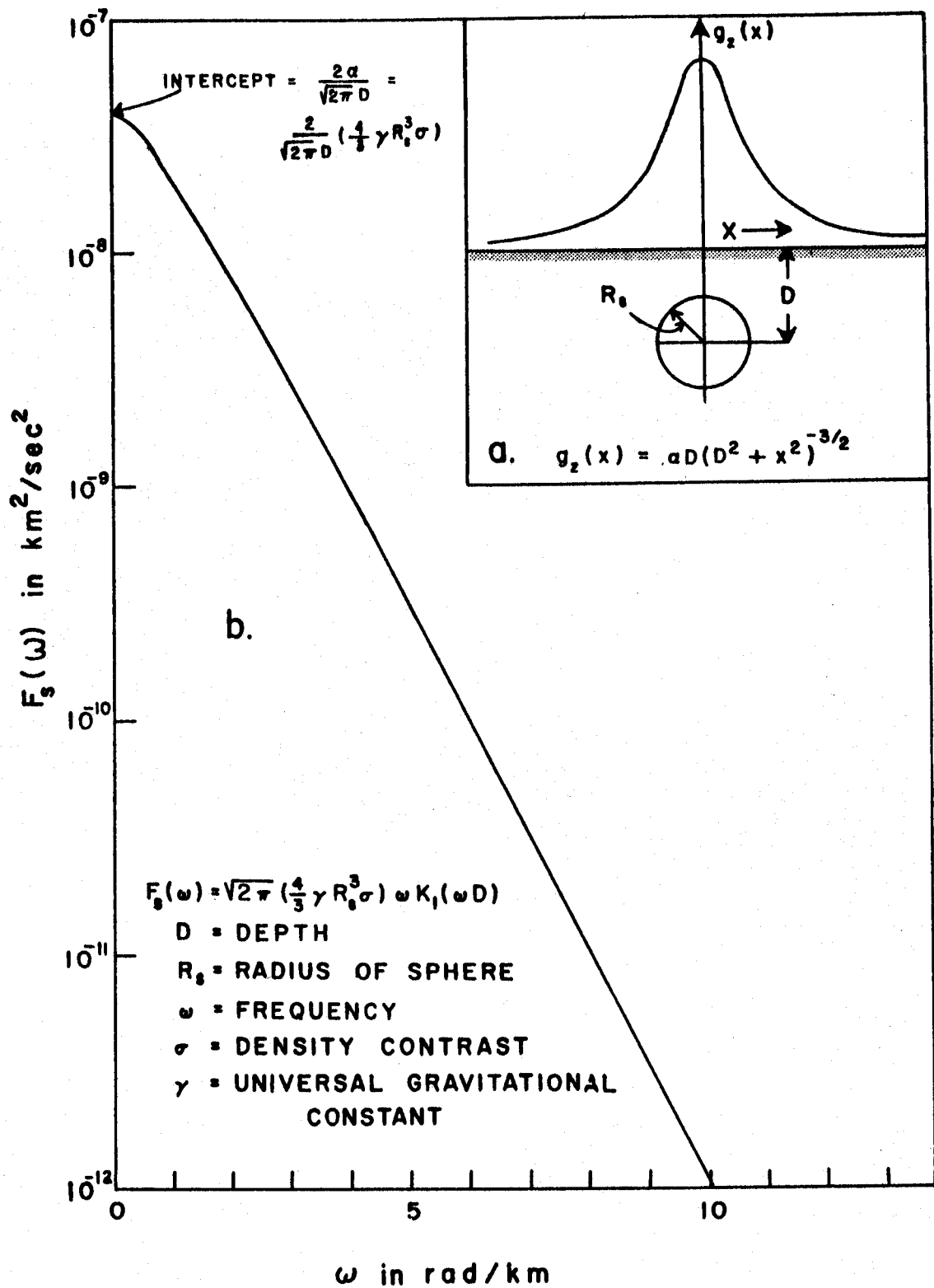


Figure 2a. Vertical gravity, $g_z(X)$, over sphere vs distance, X .
 Figure 2b. Fourier transform of vertical gravity of sphere, $F_s(\omega)$, vs frequency, ω .

Where $\alpha = 4/3\pi\gamma R_s^3\sigma$, R_s is the radius of the sphere. The other constants were defined previously. Since the vertical gravity for the sphere is an even function, the Fourier Transform is given by

$$F_s(\omega) = \frac{2\alpha D}{\sqrt{2\pi}} \int_0^\infty (D^2 + \varphi^2)^{-3/2} \cos(\omega\varphi) d\varphi \quad (8)$$

Integration yields (see Appendix B)

$$F_s(\omega) = \frac{2\alpha\omega}{\sqrt{2\pi}} K_1(\omega D) \quad (9)$$

Where $K_1(\omega D)$ is the first order, modified Bessel Function of the second kind.

Although the Fourier Transform for the sphere is not the same as that for the cylinder, it is similar and does approach an exponential as ω becomes large. A plot of the exact integral, $F_s(\omega)$, versus frequency, ω , on a semilogarithmic scale is shown in Figure 2b.

Equation (9) could not be reduced to a simple formulation of the variables, so the function was approximated by

$$F_{SA}(\omega) = \exp(A_0 + A_1\omega + A_2\omega^2) \quad (10)$$

Numerical values of $F_s(\omega)$ were calculated for different frequencies, ω , and for different depths of burial, D , for the sphere. This was done using the tables for modified Bessel Functions by Sibagaki (1955). A sequence of values of $F_s(\omega)$ for different frequencies but for the same depth of burial were fitted by the exponential in Equation (10) to determine the exponents. This was done using the method of least squares. The process was repeated for different depths of burial, thus determining the exponents as functions of

depth of burial of the sphere.

The evaluation of the exponents A_0 , A_1 , and A_2 was divided into two cases: (1) depths less than 2 km, and (2) depths greater than 1 km. This was done on the basis of depth of burial and of maximum frequency used in the determination of values of $F_s(\omega)$ for the approximation. This is illustrated by Figure 3. If the depth of burial was less than two kilometers (solid line in Figure 3), the maximum frequency used in the calculation of data points was ten radians per kilometer. If the depth of burial was greater than one kilometer (dashed line in Figure 3), the depth of burial times the maximum frequency was not allowed to exceed 25 radians. Although the above criteria seem to be arbitrary, actual data obtained by doing the transform numerically would, in general, have limits of reliability which correspond to the limits set above.

Figures 4a and 4b give the constants A_1 and A_2 for depths less than two kilometers, and Figures 4c and 4d give them for depths greater than one kilometer.

The series expansion of $F_s(\omega)$ was evaluated at $\omega = 0$ to obtain

$$F_s(0) = \frac{2\alpha}{\sqrt{2\pi} D} \quad (11)$$

This intercept is approximated by

$$e^{A_0} = F_{sA}(0) \cong F_s(0) \quad (12)$$

Figure 5 gives the ratio, λ , of the approximate intercept, $F_{sA}(0)$, and the theoretical intercept, $F_s(0)$. $\lambda = F_s(0)/F_{sA}(0)$.

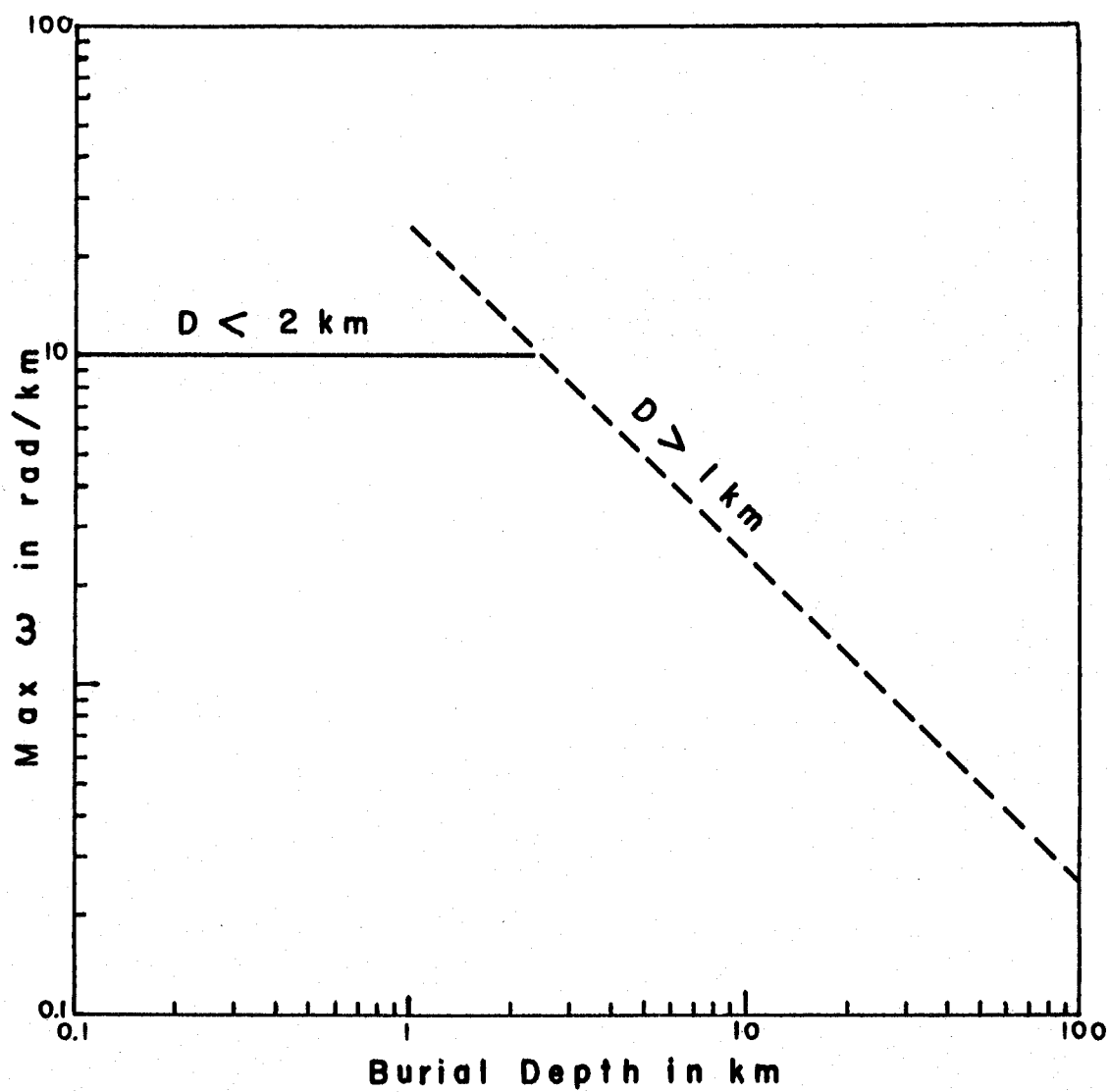


Figure 3. Maximum frequency used in approximation vs depth of burial, D .

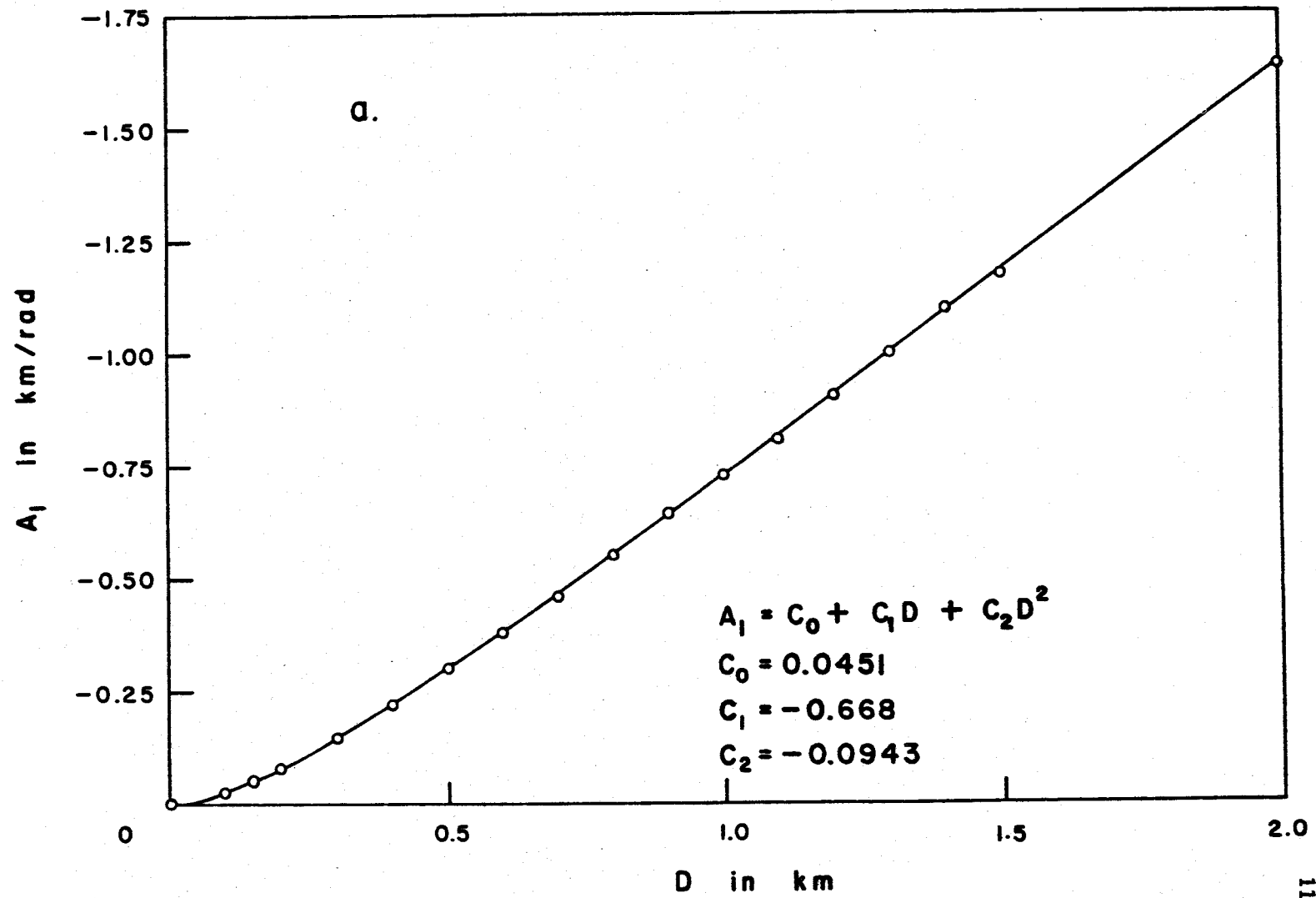


Figure 4a. Approximation constant, A_1 , vs depth, D , for depths less than 2 km.

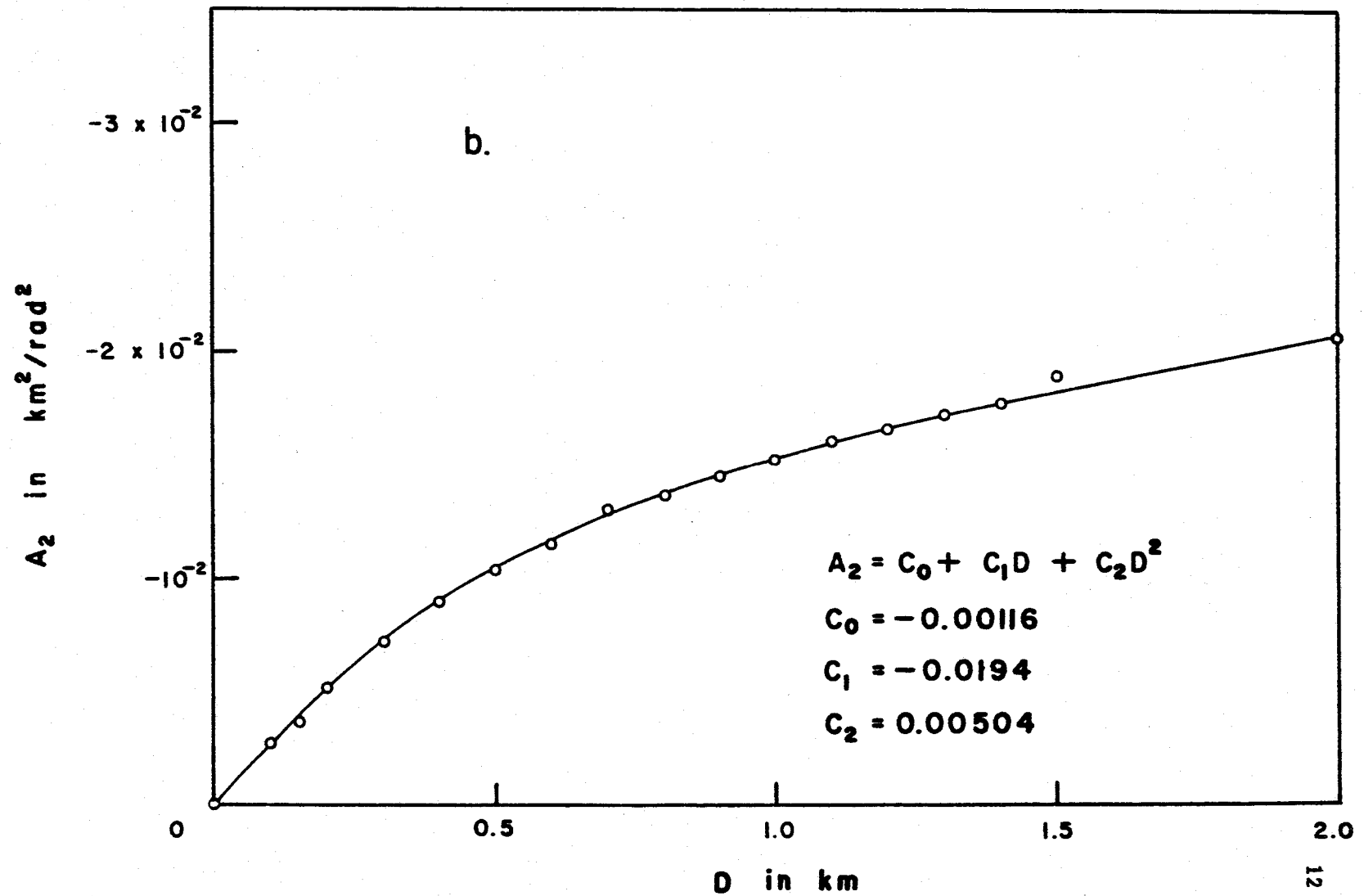


Figure 4b. Approximation constant, A_2 , vs depth, D , for depths less than 2 km.

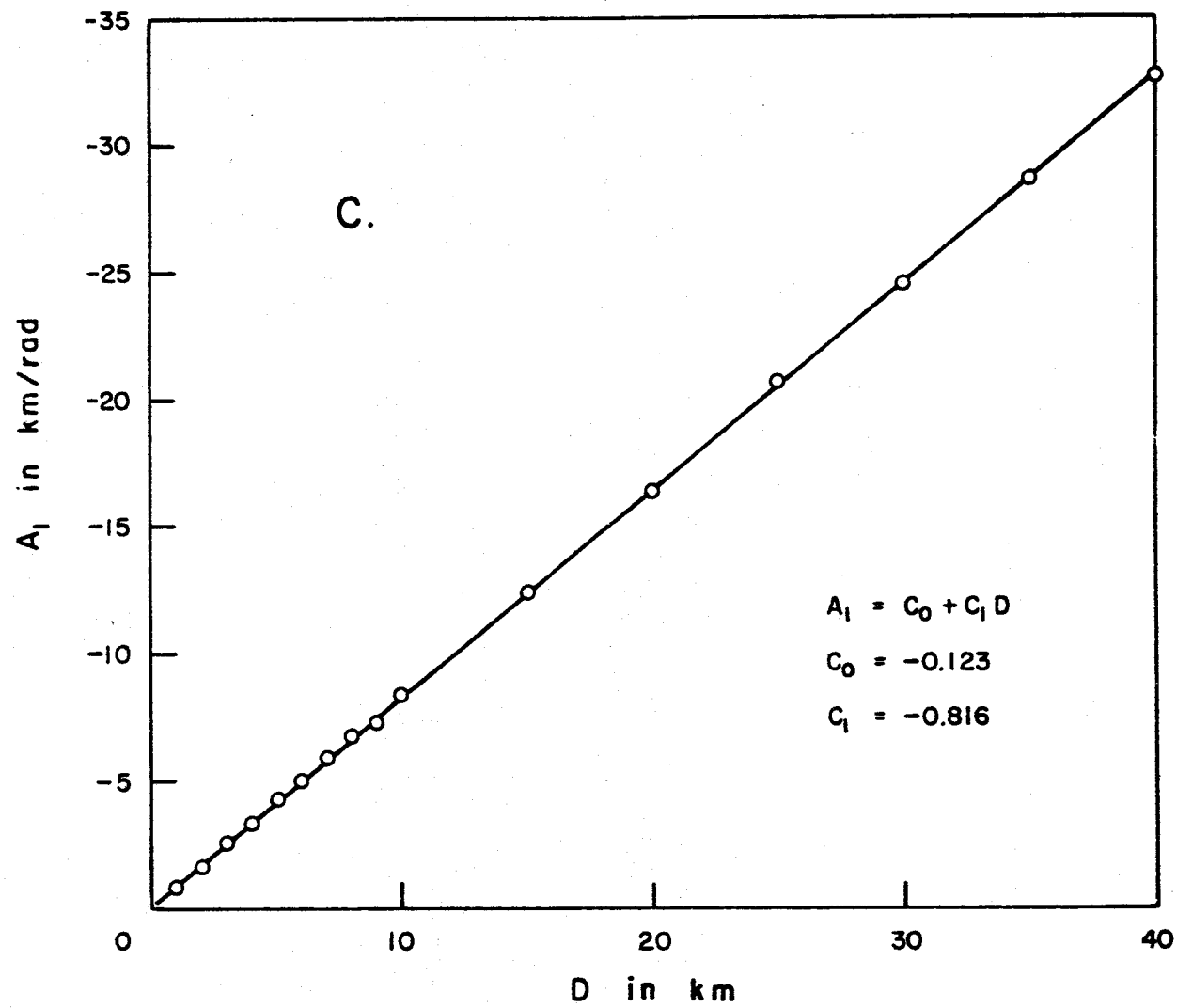


Figure 4c. Approximation constant, A_1 , vs depth, D , for depths greater than 1 km.

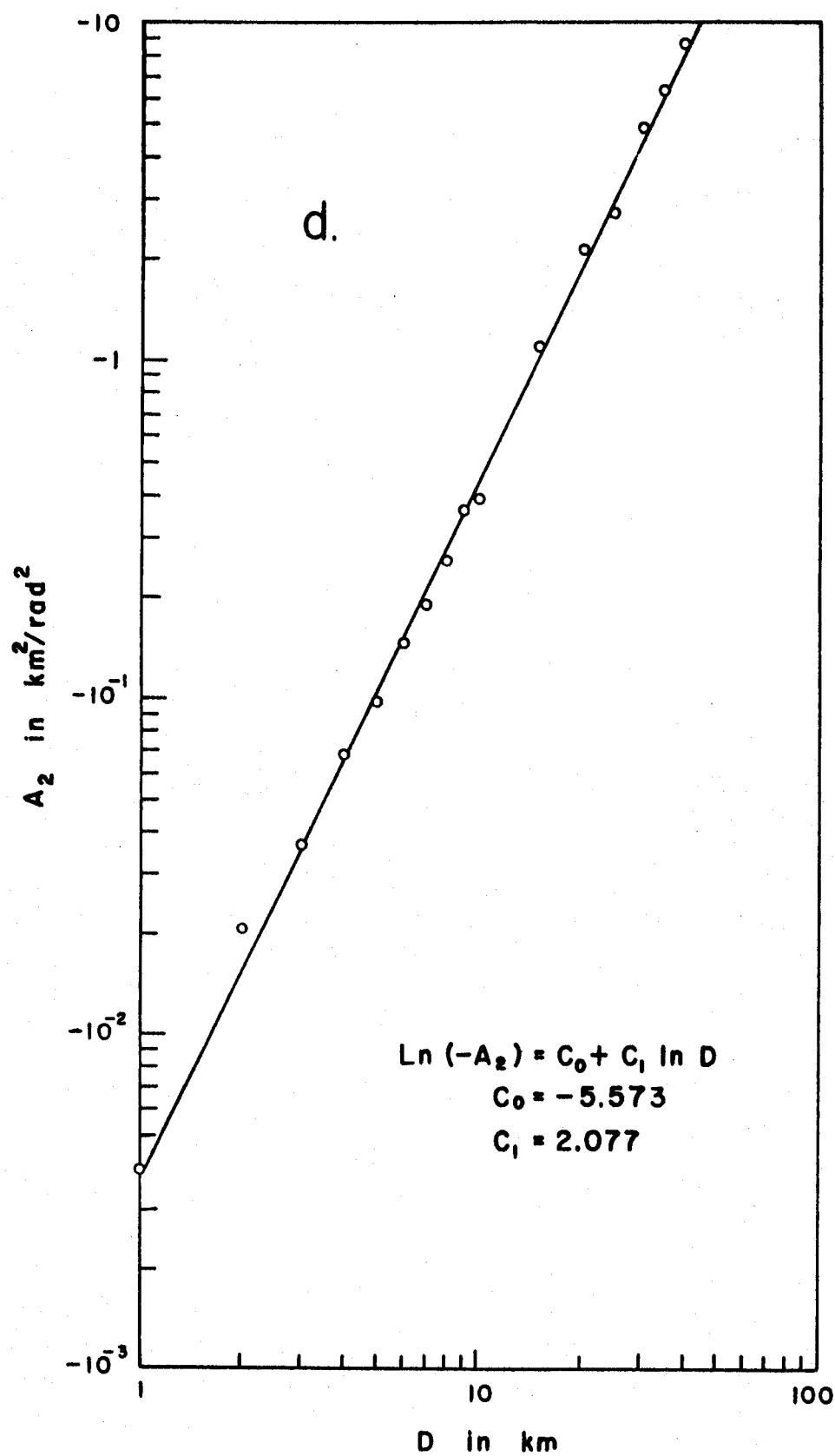


Figure 4d. Approximation constant, A_2 , vs depth, D , for depths greater than 1 km.

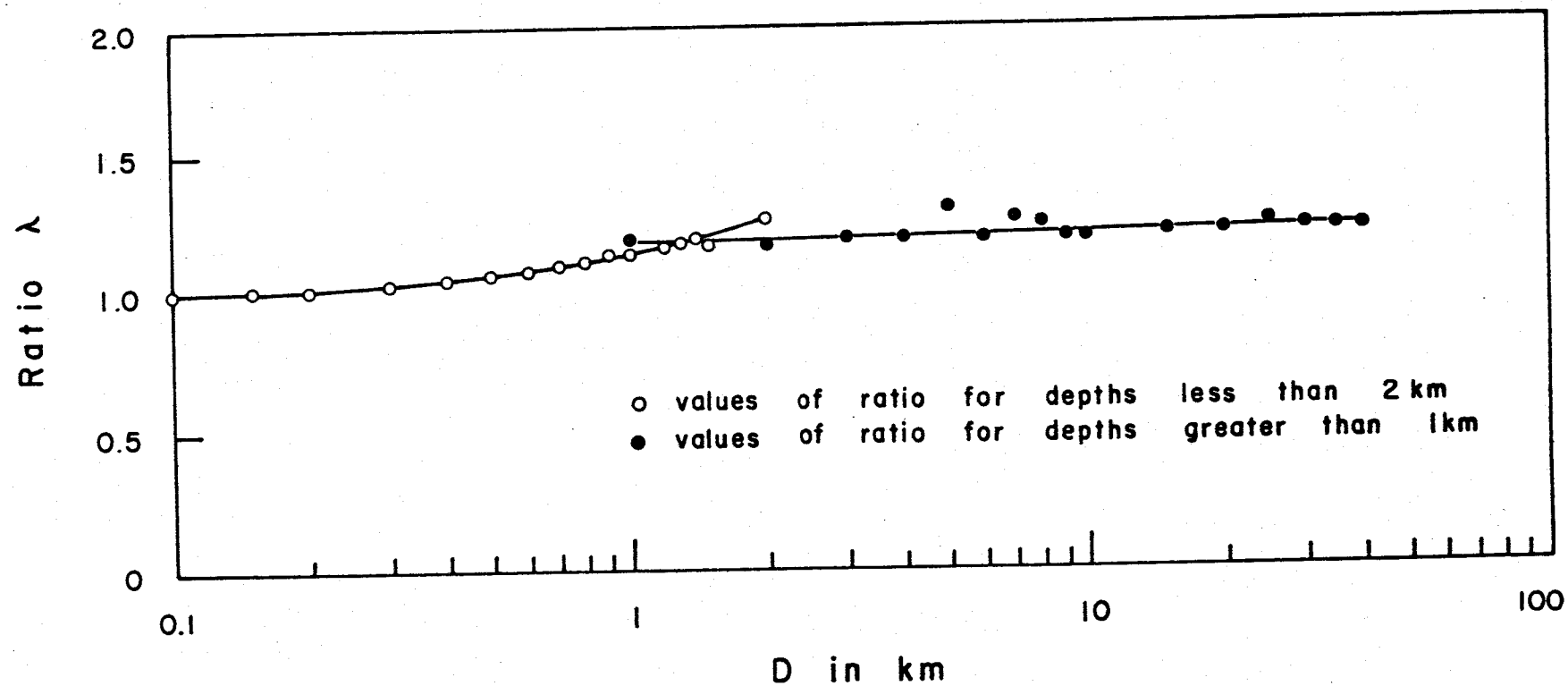


Figure 5. Ratios of approximate intercept, $F_{SA}(0)$, to actual intercept, $F_S(0)$, of Fourier transform of vertical gravity of sphere.

In order to use the intercept to determine size and density of a sphere, it is necessary to correct the intercept of the approximate relationship by using the ratios given in Figure 5. For example, if the transform of a sphere is approximated and it is found that $A_0 = -16.30$, $A_1 = -2.57$, and $A_2 = -0.0364$, then from Figures 4c and 4d it is found that the depth is 3.00 kilometers. Using the value of the ratio, λ , for this depth from Figure 5, the actual intercept is found to be

$$F_s(0) = \lambda e^{A_0} = 1.20 \times 8.33 \times 10^{-8} = 1.00 \times 10^{-1} \text{ km}^2/\text{sec}^2$$

Substituting this value for $F_s(0)$ into Equation (11),

$$\alpha = 3.76 \times 10^{-7} \text{ km}^3/\text{sec}^2$$

Using the definition of α given by Equation (7)

$$\sigma R_s^3 = 1.34 \times 10^{12} \text{ kg}$$

This gives the relative size of the sphere. (Units used in this research were the kilometer, kilogram, and second.)

(c) Fault

The vertical gravity at each point along a profile perpendicular to the strike of a fault (Figure 6a) is given by

$$g_z(X) = 2\delta\sigma \left(\frac{X}{2} \ln \left[\frac{X^2 + D^2}{X^2 + (D+T)^2} \right] + \frac{\pi T}{2} + D \tan^{-1} \left(\frac{X}{D} \right) - (D+T) \tan^{-1} \left(\frac{X}{D+T} \right) \right) \quad (13)$$

Where T is the throw of the fault. The other variables were defined previously.

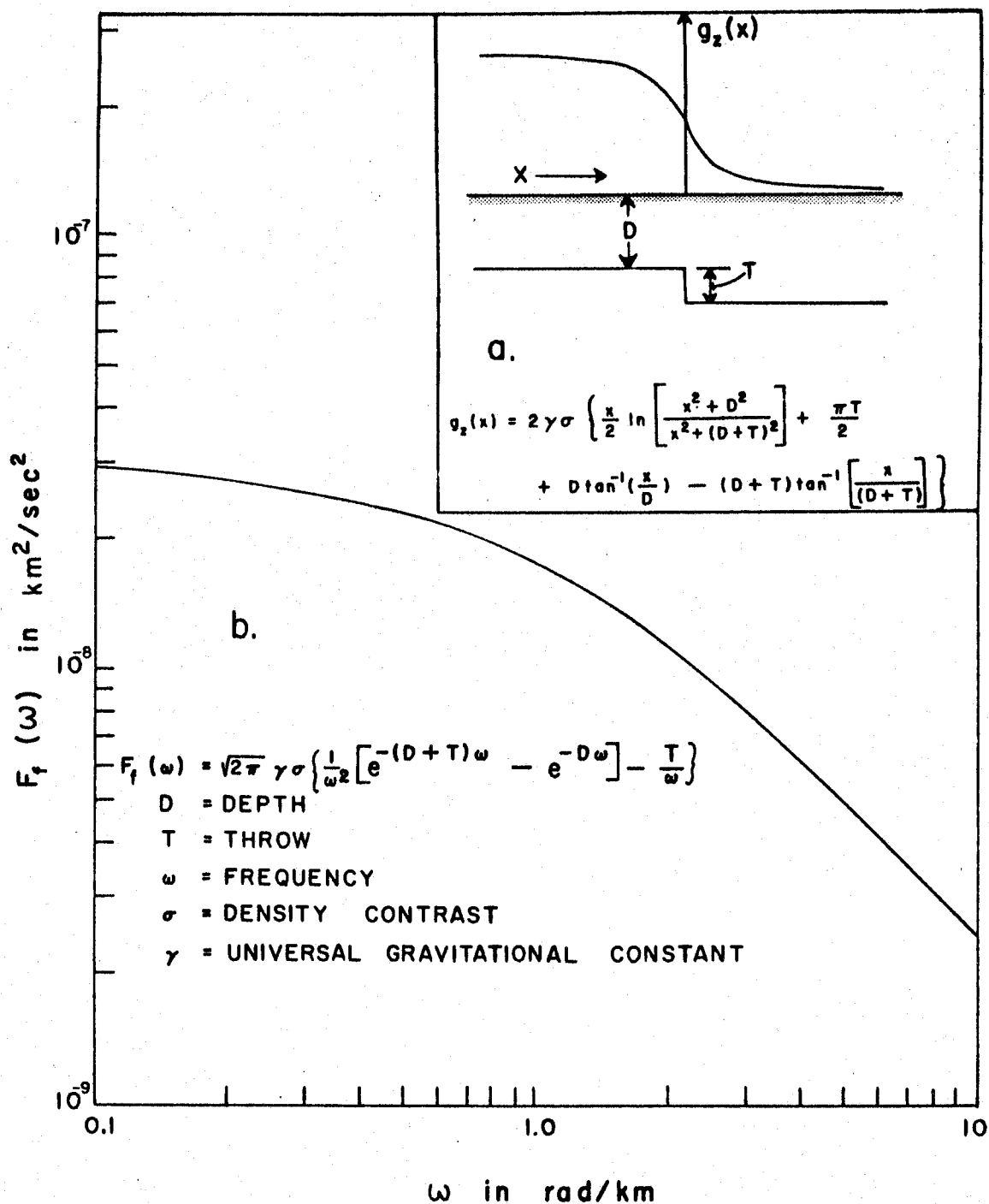


Figure 6a. Vertical gravity over fault, $g_z(X)$, vs distance, X .

Figure 6b. Fourier transform, $F_f(\omega)$, of vertical gravity over fault vs frequency, ω .

The vertical gravity for the fault is an odd function
 $[f(X) = -f(-X)]$, so the Fourier Transform is given by (see Appendix B)

$$F_f(\omega) = \frac{2}{\sqrt{2\pi}} \int_0^{\infty} g_z(\phi) \sin(\omega\phi) d\phi \quad (14)$$

In Appendix B this integral is shown to be

$$F_f(\omega) = \sqrt{2\pi} \gamma \sigma \left(1/\omega^2 \left[e^{-(D+T)\omega} - e^{-D\omega} \right] + T/\omega \right) \quad (15)$$

A plot of the exact integral, $F_f(\omega)$, versus frequency, ω , on a logarithmic scale is shown in Figure 6b.

Multiplying Equation (15) by ω gives

$$f(\omega) = \omega F_f(\omega) = 2\pi \gamma \sigma \left(1/\omega \left[e^{-(D+T)\omega} - e^{-D\omega} \right] + T \right) \quad (16)$$

The limit, $\lim_{\omega \rightarrow \infty} f(\omega) = \sqrt{2\pi} \gamma \sigma T$, is approached rapidly (Figure 6c) so it can be evaluated. If this limit is subtracted from Equation (16) and the difference multiplied by ω , Equation (17) is derived.

$$G(\omega) = \sqrt{2\pi} \gamma \sigma \left[e^{-(D+T)\omega} - e^{-D\omega} \right] \quad (17)$$

A plot of $G(\omega)$ versus frequency on a semilogarithmic scale is shown in Figure 6d. The depth, D , and throw, T , can be obtained by analyzing the reduced transform, $G(\omega)$, in terms of the sum of two exponentials analogous to the analysis of multiple decay spectra.

For a description of this method see Kaplan (1955).

In essence, this method involves fitting an exponential to the linear portion of the curve plotted on a semilogarithmic scale (line A, Figure 6d). This exponential is subtracted from the total spectrum and the residue is replotted. An exponential is fitted to

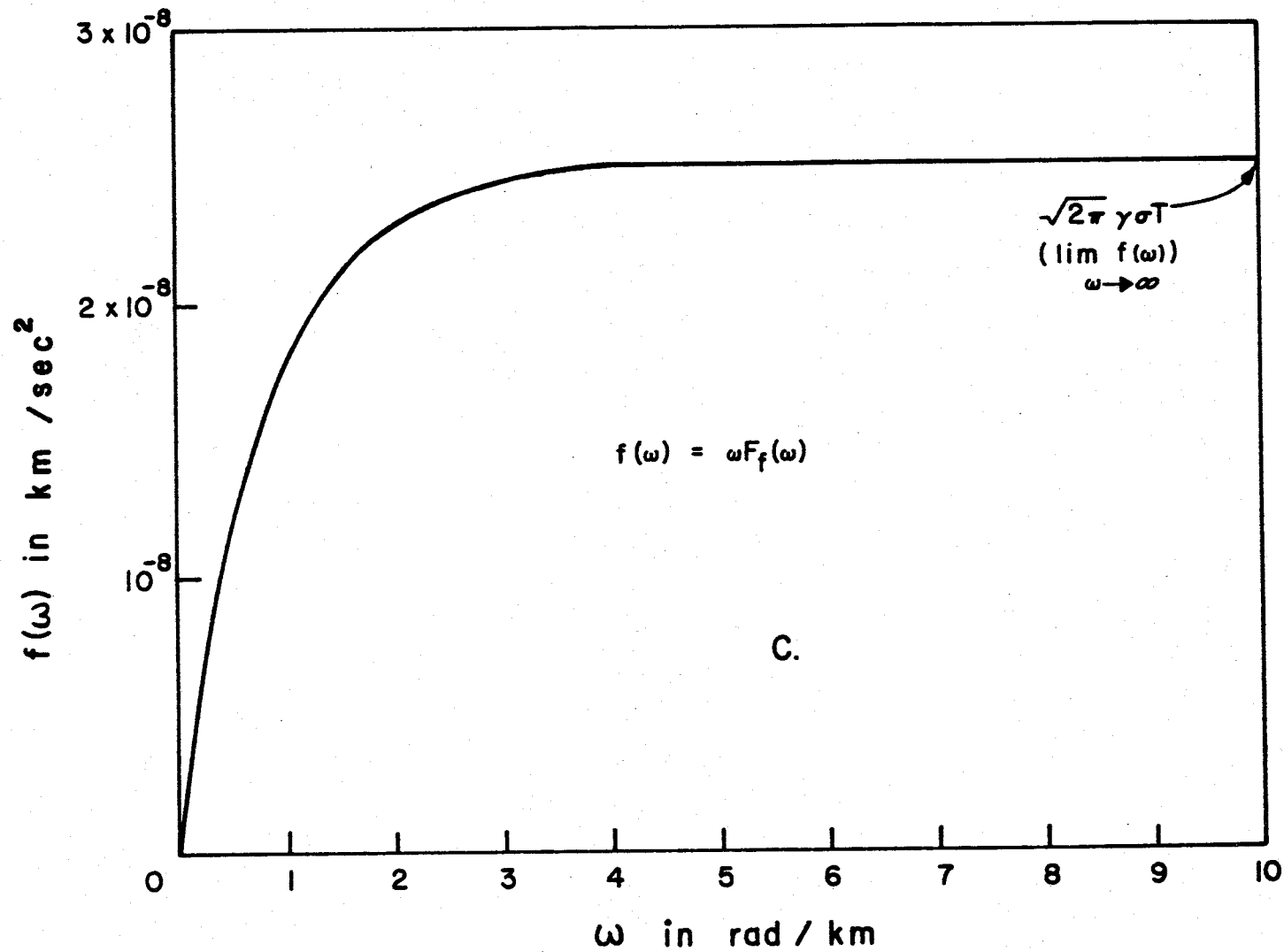


Figure 6c. Modified Fourier Transform, $f(\omega)$, $[f(\omega) = \omega F_f(\omega)]$ vs frequency to determine $\sqrt{2\pi} \gamma \sigma T$.

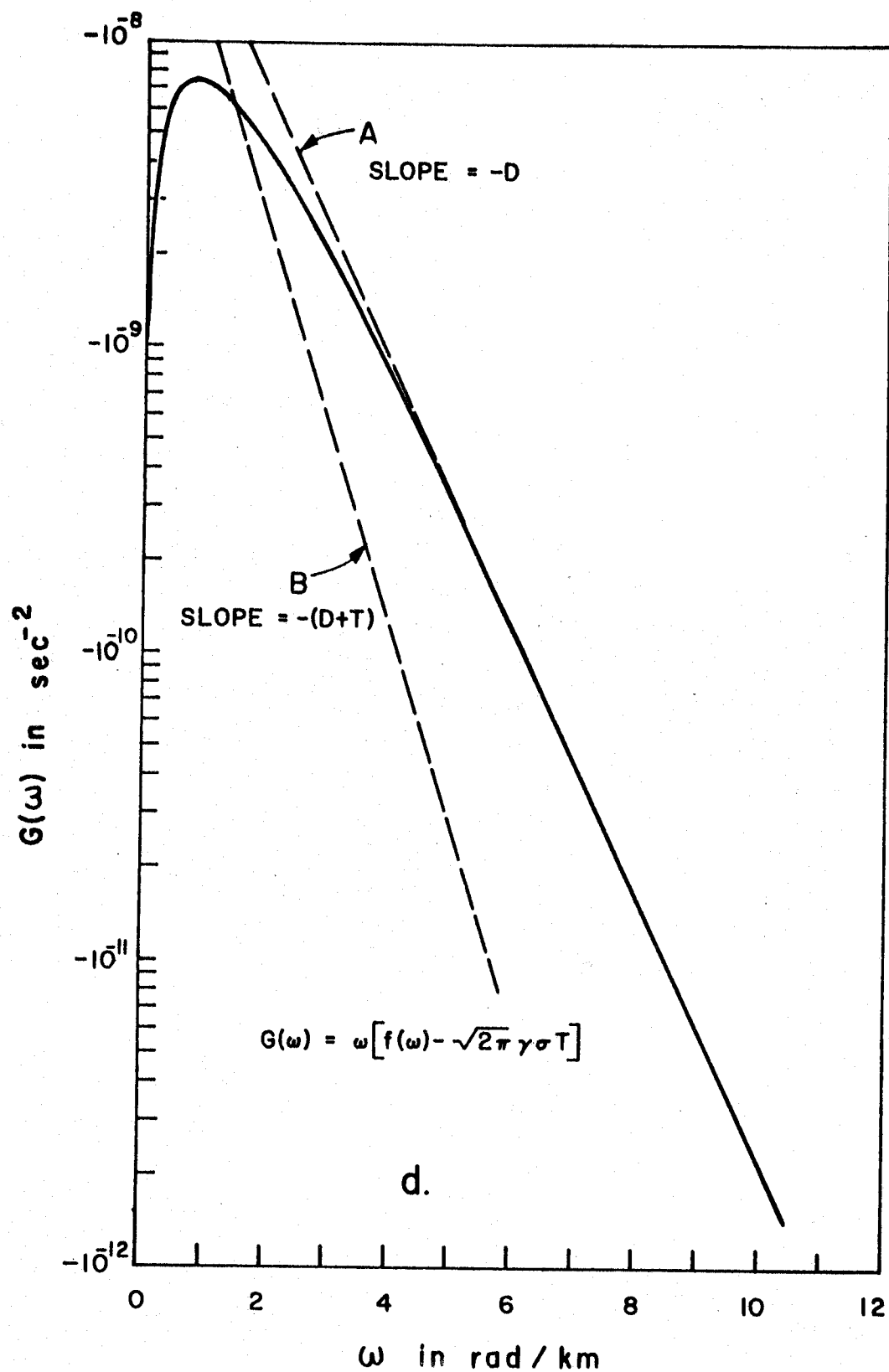


Figure 6d. Reduced Fourier Transform, $G(\omega)$, vs frequency, ω , used to determine depth and throw of fault.

the linear portion of the new set of data (line B, shown as a negative plot in Figure 6d). The slopes of lines A and B are equal to $-D$ and $-(D+T)$ respectively. Knowing the throw, the density contrast can be found from the limit of $f(\omega)$.

II. Transforms and Analysis of More Complex Structures

The anomaly due to two cylinders at different depths was analyzed for the size and depth information for each cylinder in order to test resolution and accuracy of the method with respect to depth. The anomaly due to a cylinder separated horizontally from, and deeper than, a fault located at depth was analyzed to test resolution with respect to the type of body. These cases were tested by doing numerical integrations of the digitized theoretical anomalies. The computer program used to do the numerical transform is described in Appendix C.

(a) Multiple Cylinders

Figure 7a shows the calculated gravity anomaly due to two cylinders in a vertical plane at different depths. The open circles in Figure 7b are values of the Fourier Transform, obtained by numerical integration, versus frequency on a semilogarithmic scale. Since the Fourier Transform is the sum of two exponentials (see Equation (3)), this spectrum was analyzed by using the method of multiple decay spectra analysis described in section 1c. Thus, the slopes of lines A and B shown in Figure 7b are the depths of the cylinders. The intercepts of these lines are related to the sizes

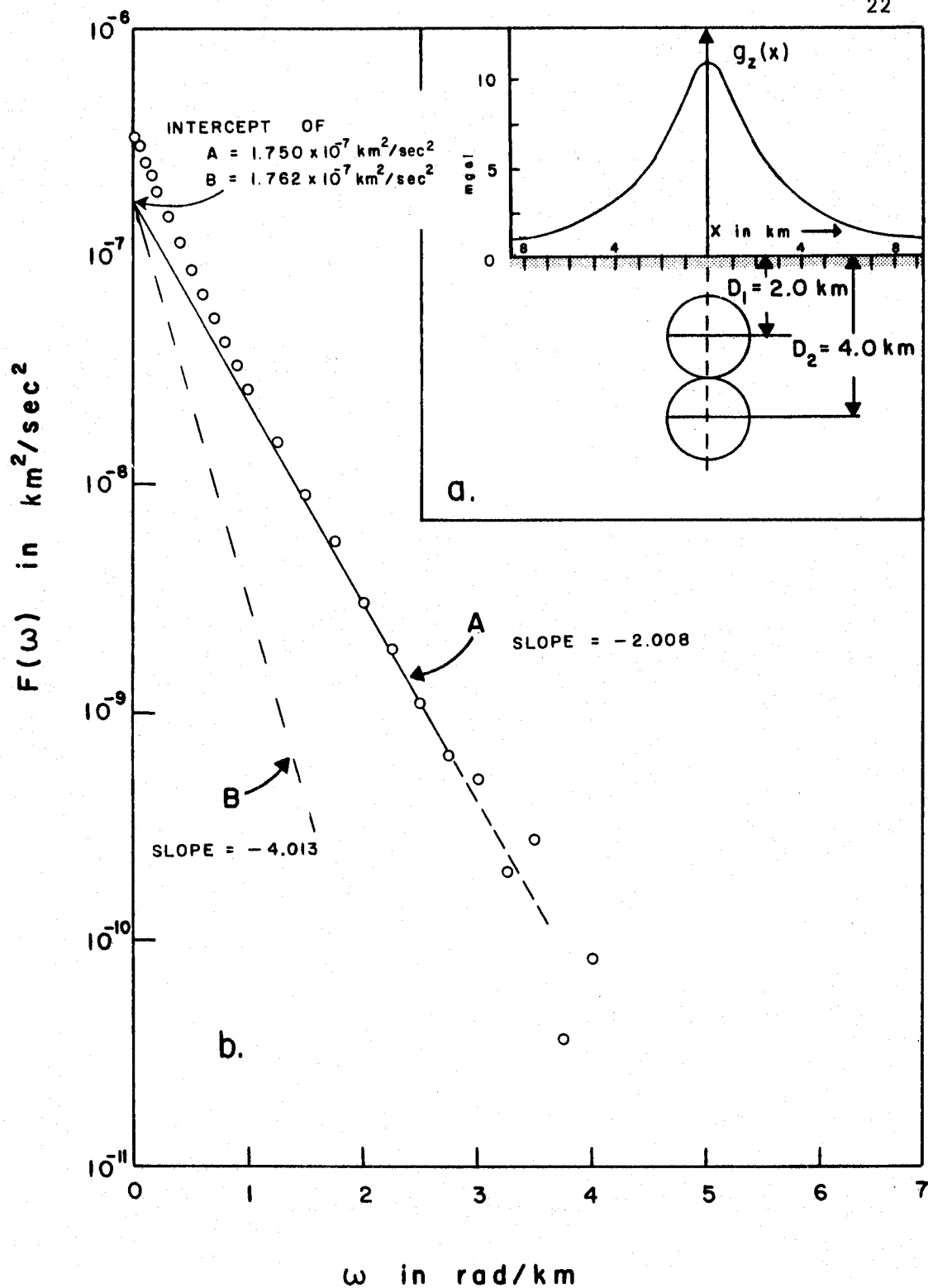


Figure 7a. Calculated vertical gravity over two infinite horizontal cylinders vs distance, x .

Figure 7b. Fourier transform, $F(\omega)$, of calculated vertical gravity over two infinite horizontal cylinders vs frequency, ω .

of the cylinders by Equation (6).

This method has been used in resolving three cylinders successfully. However, statistical methods of analysis will probably be needed to obtain maximum resolution with more than two cylinders, since numerical approximations used in the analysis begin to show as scatter of data points.

(b) Cylinder-Fault

Figure 8a shows the calculated gravity anomaly over a cylinder and a fault. The cylinder is located below the fault and offset from it by a distance Y as shown on the diagram.

Since the anomaly due to the cylinder is even and that due to the fault is odd, the total transform can be written as (see Appendix A)

$$\begin{aligned} F(\omega) &= e^{i\omega Y} F_1(\omega) + iF_2(\omega) \\ &= \cos(\omega Y)F_1(\omega) + i[\sin(\omega Y)F_1(\omega) + F_2(\omega)] \end{aligned} \quad (18)$$

Where $F_1(\omega)$ (even function) is the transform for the anomaly of the cylinder and $F_2(\omega)$ (odd function) is the transform for the anomaly of the fault. The exponential term, $e^{i\omega Y}$, is due to the cylinder being offset horizontally a distance Y from the throw of the fault (Figure 8a).

The Fourier transform of the total anomaly was obtained by numerical integration and separated into the real and imaginary parts. The horizontal separation distance, Y , was found by determining the zeros of the real part of the transform, $\cos(\omega Y)F_1(\omega)$. These zeros

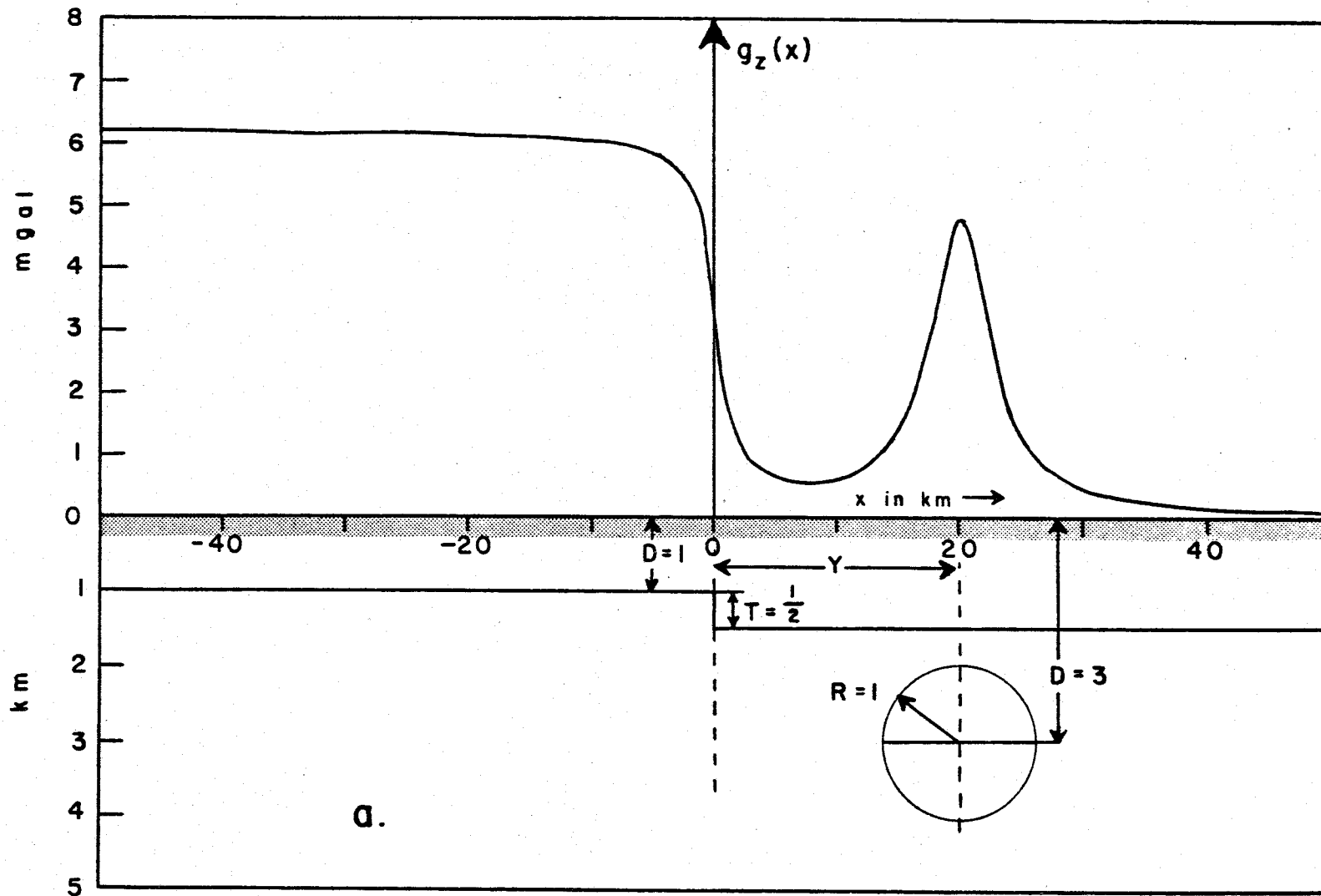


Figure 8a. Calculated vertical gravity over fault and cylinder offset from fault by distance, Y .

are at intervals of $\omega = \pi/Y$.

The real part of $F(\omega)$ was divided by $\cos(\omega Y)$ to obtain $F_1(\omega)$. Figure 8b shows $F_1(\omega)$, derived from $F(\omega)$, plotted versus frequency. That plot is similar to that of the cylinder shown in Figure 1b. The curve was fitted to the data by the method of least squares which gives values for the slope (depth) and intercept (size and density), the parameters for the cylinder.

Values of $F_1(\omega)$ were calculated using the derived parameters. These values were multiplied by $\sin(\omega Y)$ and subtracted from the imaginary part of $F(\omega)$ to obtain $F_2(\omega)$. Figure 8c shows $F_2(\omega)$, derived from $F(\omega)$, plotted versus frequency. These data were analyzed by the methods described in Section Ic to find the parameters for the fault.

III. Results and Accuracy of Analysis

The results of the analysis of the two complex structures compared to the actual values of the parameters are shown in Tables I and II. Table I is this data for the multiple cylinders and Table II gives the data for the cylinder and fault.

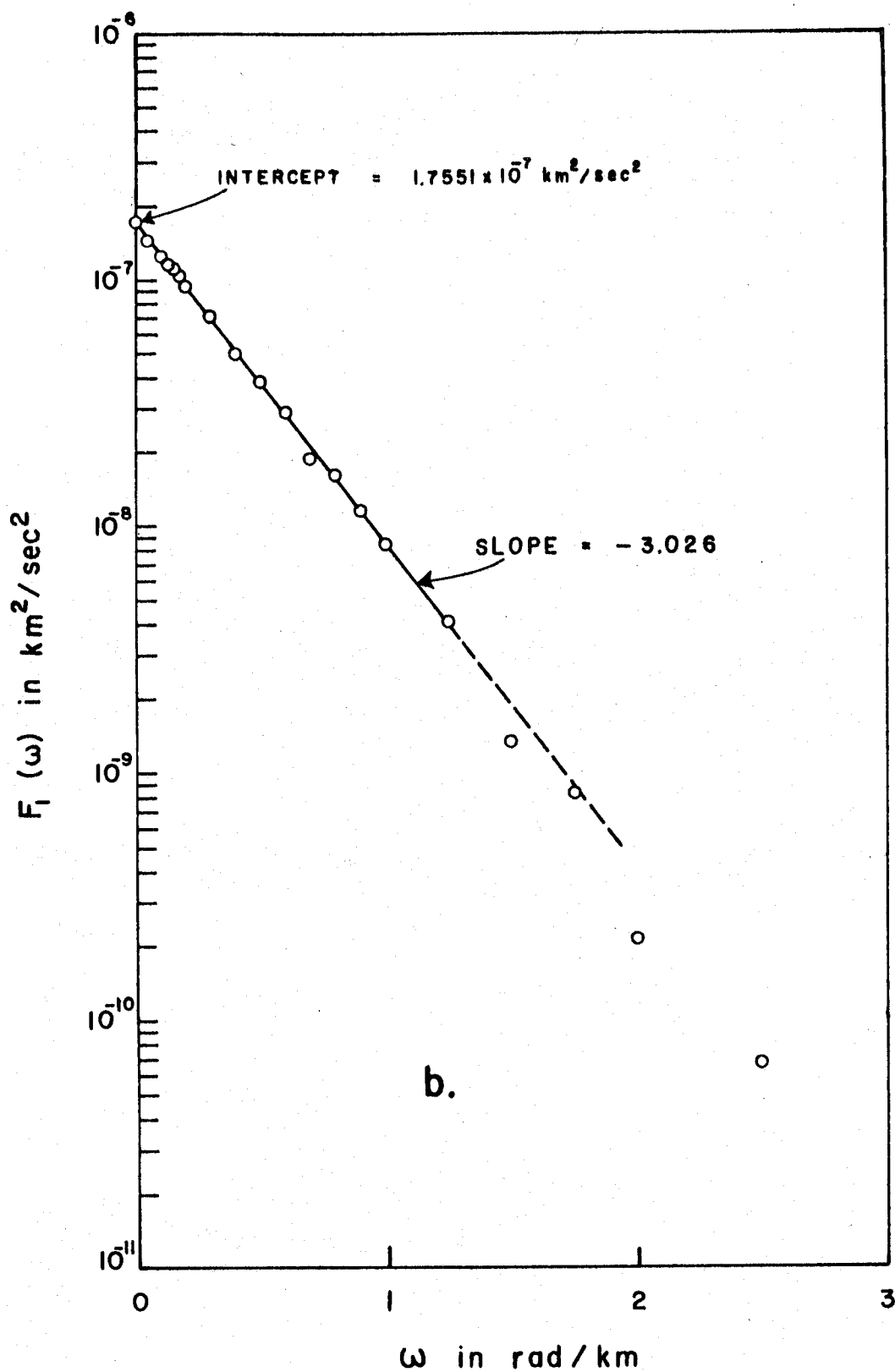


Figure 8b. Fourier transform of cylinder extracted from total calculated Fourier transform by considering only real parts of the total calculated transform.

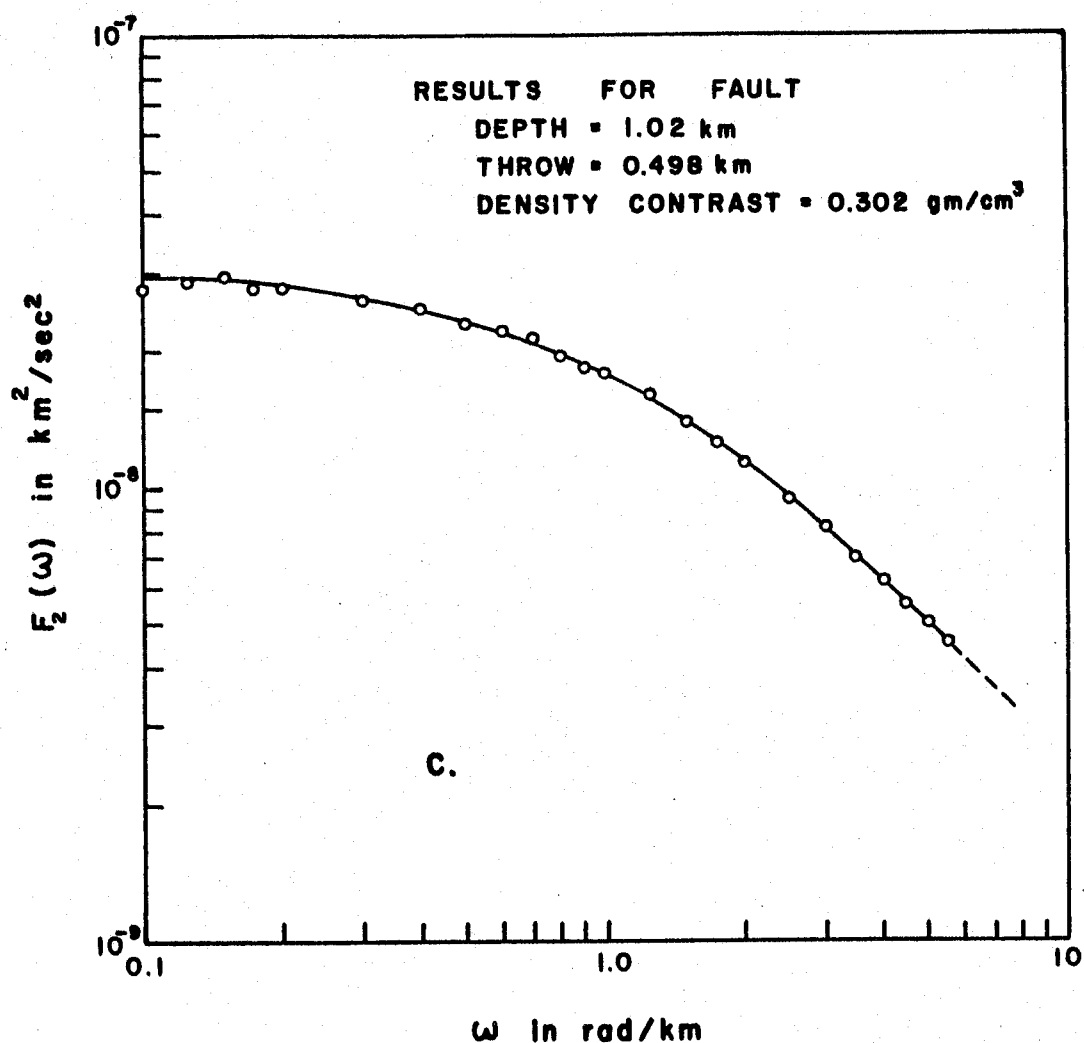


Figure 8c. Fourier Transform of fault extracted from the total calculated Fourier Transform by the real part (transform of cylinder) from the total calculated transform.

Table I. Computed and Actual Data for Multiple Cylinders

Actual Depths (km)	Cal. Depths (km)	% Error	Actual Intercept (km^2/sec^2)	Calculated Intercept (km^2/sec^2)	% Error
2	2.008	0.4	1.751×10^{-7}	1.750×10^{-7}	0.1
4	4.013	0.4	1.751×10^{-7}	1.762×10^{-7}	0.6

Table II. Computed and Actual Data for Cylinder and Fault

Cylinder								
Actual Depths (km)	Cal. Depths	% Error	Actual Intercept (km ² /sec ²)			Calculated Intercept (km ² /sec ²)		% Error
3.000	3.026	0.87	1.7514 x 10 ⁻⁷			1.7551 x 10 ⁻⁷		0.21
Fault								
Actual Depth (km)	Calc. Depth (km)	% Error	Actual Throw (km)	Calc. Throw (km)	% Error	Actual Density Contrast (gm/cc)	Calc. Density Contrast (gm/cc)	% Error
1.00	1.02	2.0	0.500	0.498	0.4	0.300	0.302	0.7

In the cases of the simple structures, numerical analysis has also been performed and errors are on the order of one-tenth of one percent for the determination of the parameters of the bodies.

SUMMARY AND CONCLUSIONS

It has been shown that a Fourier Integral method of analysis can be of value in the analysis of theoretical subsurface structures. In the case of the cylinder and sphere the depth and relative size can be determined. For the fault the depth, throw, and density contrast can be determined uniquely.

It has also been shown in sections II(a) and II(b) that this method is capable of separating more complex structures into their simpler components.

In theory there is no limit to the accuracy, provided the anomalies are produced by perfect simple bodies. The limit on the accuracy of the analyses presented in this thesis was only dependent upon the accuracy of the method of integration to find the transform. These errors are discussed in Appendix C.

The applicability of this method to the analysis of the gravity anomalies of actual geological structures remains to be demonstrated. Current research is being directed toward this end.

BIBLIOGRAPHY

1. Dean, W. C. Frequency analysis for gravity and magnetic interpretation. *Geophysics* 23(1):97-127. 1958.
2. Dewight, H. B. Tables of integrals and other mathematical data. 4th ed. New York, MacMillan, 1961. 336 p.
3. Fizeau, H. *Annalen der Chemie und Physik* 3(66):429. 1862.
4. Hurwitz, H. Jr. and P. F. Zweifel. Numerical quadrature of Fourier transform integrals. *Mathematical Tables and Other Aids to Computation* 10(55):140-149. 1956.
5. Kaplan, I. Nuclear physics. Reading, Addison-Wesley, 1955. 333p.
6. Milne, W. E. Numerical calculus. Princeton, Princeton University Press. 1949. 329 p.
7. Nettleton, L. L. Geophysical prospecting for oil. New York, McGraw Hill, 1940. 275 p.
8. Peters, L. J. The direct approach to magnetic interpretation and its practical applications. *Geophysics* 14(3):290-320. 1949.
9. Sibagaki, W. 0.01% tables of modified Bessel functions. Tokyo, Baifukan, 1955. 147 p.
10. Solo'yev, O. A. Use of the frequency method for the determination of some parameters of magnetic bodies. *Akademiia Nauk SSSR Sibirskoy Otdeleniye, Geologiya i Geofizika* 2:122-125. 1962.
11. Tomoda, Y. and K. Aki. Use of the function $\sin(x)/x$ in gravity problems. *Proceedings of the Japan Academy of Tokyo* 31:443-448. 1955.
12. Tsuboi, C. and T. Fuchida. Relation between gravity anomalies and the corresponding subterranean mass distribution. *Bulletin of the Earthquake Research Institute, Tokyo Imperial University* 16(23):273-283. 1938.

APPENDICES

APPENDIX A

Some Properties of the Fourier Integral

If a function $f(x)$ is piecewise smooth in every finite interval and assumes the value of the mean of the left and right hand limits at all discontinuities, and further if the integral $\int_{-\infty}^{\infty} |f(x)| dx$ exists, then the Fourier Integral Theorem states that

$$f(x) = \frac{1}{2\pi} \int_{-\infty}^{\infty} d\omega \int_{-\infty}^{\infty} f(t) e^{i\omega(t-x)} dt$$

For a real function this may also be written

$$f(x) = \frac{1}{\pi} \int_0^{\infty} d\omega \int_{-\infty}^{\infty} f(t) \cos \omega(t-x) dt$$

This formula may be written as two reciprocal functions. Setting

$$F(\omega) = \frac{1}{\sqrt{2\pi}} \int_{-\infty}^{\infty} f(x) e^{i\omega x} dx$$

then

$$f(x) = \frac{1}{\sqrt{2\pi}} \int_{-\infty}^{\infty} F(\omega) e^{-i\omega x} d\omega$$

$F(\omega)$ is called the Fourier Transform of $f(x)$. Further, if $f(x)$ is a real and even function,

$$F(\omega) = \sqrt{\frac{2}{\pi}} \int_0^{\infty} f(x) \cos(\omega x) dx \qquad f(x) = \sqrt{\frac{2}{\pi}} \int_0^{\infty} F(\omega) \cos(\omega x) d\omega$$

or if $f(x)$ is a real and odd function

$$F(\omega) = \sqrt{\frac{2}{\pi}} \int_0^{\infty} f(x) \sin(\omega x) dx \qquad f(x) = \sqrt{\frac{2}{\pi}} \int_0^{\infty} F(\omega) \sin(\omega x) d\omega$$

Displacement Theorem

For a function $f(x)$ displaced by an amount z from the origin, the Fourier Transform is given by

$$G(\omega) = \frac{1}{\sqrt{2\pi}} \int_{-\infty}^{\infty} f(x-z) e^{i\omega x} dx$$

Changing the variable of integration to $y = x-z$, $dy = dx$, the transform becomes

$$\begin{aligned} G(\omega) &= \frac{1}{\sqrt{2\pi}} \int_{-\infty}^{\infty} f(y) e^{i\omega(y+z)} dy \\ &= \frac{1}{\sqrt{2\pi}} e^{i\omega z} \int_{-\infty}^{\infty} f(y) e^{i\omega y} dy \end{aligned}$$

So that for a function displaced by an amount z from the origin, the Fourier Transform is

$$G(\omega) = e^{i\omega z} F(\omega)$$

where

$$F(\omega) = \frac{1}{\sqrt{2\pi}} \int_{-\infty}^{\infty} f(x) e^{i\omega x} dx$$

is the Fourier Transform of $f(x)$.

APPENDIX B

Integration of the Sphere and Fault Transforms(a) Sphere

The Fourier Transform of the vertical gravity over a buried sphere is given by (Equation (6), Section Ib)

$$F_s(\omega) = \frac{2\alpha D}{\sqrt{2\pi}} \int_0^\infty (D^2 + \varphi^2)^{-3/2} \cos(\omega\varphi) d\varphi$$

This is not readily integrable; however, the tables (Dewight, 1961) give

$$\int_0^\infty (D^2 + \varphi^2)^{-1/2} \cos(\omega\varphi) d\varphi = K_0(\omega D)$$

where $K_0(\omega D)$ is the zero order, modified Bessel Function of the second kind. Using Leibnitz' rule this gives

$$\frac{\partial}{\partial D} \int_0^\infty (D^2 + \varphi^2)^{-1/2} \cos(\omega\varphi) d\varphi = \frac{\partial}{\partial D} K_0(\omega D)$$

or

$$-D \int_0^\infty (D^2 + \varphi^2)^{-3/2} \cos(\omega\varphi) d\varphi = -\omega K_1(\omega D)$$

Which gives for the transform

$$F_s(\omega) = \frac{2\alpha\omega}{\sqrt{2\pi}} K_1(\omega D)$$

where $K_1(\omega D)$ is the first order, modified Bessel Function of the second kind.

(b) Fault

The vertical gravity along a profile perpendicular to the strike of a vertical fault is given by (Equation (13), Section Ic)

$$g_z(x) = 2\gamma\sigma \left(\frac{x}{2} \ln \left[\frac{x^2 + D^2}{x^2 + (D+T)^2} \right] + \frac{\pi T}{2} + D \tan^{-1} \left(\frac{x}{D} \right) - (D+T) \tan^{-1} \left[\frac{x}{(D+T)} \right] \right)$$

Using the transformation

$$\tan^{-1}(x/a) = \frac{\pi}{2} - \tan^{-1} \left(\frac{a}{x} \right)$$

This Equation becomes

$$g_z(x) = 2\gamma\sigma \left(\frac{x}{2} \ln \left[\frac{x^2 + D^2}{x^2 + (D+T)^2} \right] + D \tan^{-1} \left(\frac{D}{x} \right) - (D+T) \tan^{-1} \left[\frac{(D+T)}{x} \right] \right)$$

So that the Fourier Transform of $g_z(x)$ is given by

$$F_f(\omega) = \frac{2\gamma\sigma}{\sqrt{2\pi}} \int_{-\infty}^{\infty} \left(\frac{\phi}{2} \ln \left[\frac{\phi^2 + D^2}{\phi^2 + (D+T)^2} \right] + D \tan^{-1} \left(\frac{D}{\phi} \right) - (D+T) \tan^{-1} \left[\frac{(D+T)}{\phi} \right] \right) \sin(\omega\phi) d\phi \quad (1)$$

Integrating each term of the integral individually: Let

$$A = 2 \int_0^{\infty} \frac{\phi}{2} \ln \left[\frac{\phi^2 + D^2}{\phi^2 + (D+T)^2} \right] \sin(\omega\phi) d\phi$$

Integrating by parts

$$A = \frac{1}{\omega^2} \log \left[\frac{\phi^2 + D^2}{\phi^2 + (D+T)^2} \right] (\sin \omega\phi - \omega\phi \cos \omega\phi) \Big|_0^{\infty} - \frac{1}{\omega^2} \int_0^{\infty} d \left(\ln \left[\frac{\phi^2 + D^2}{\phi^2 + (D+T)^2} \right] \right) (\sin \omega\phi - \omega\phi \cos \omega\phi)$$

In the first term the limit as ϕ goes to infinity must be evaluated.

(It is easy to see that the value of the limit at $\phi = 0$ is zero.)

The only term that will give any trouble is

$$\lim_{\varphi \rightarrow \infty} \frac{\varphi}{\omega} \ln \left[\frac{\varphi^{2+D^2}}{\varphi^{2+(D+T)^2}} \right] \cos \omega \varphi \leq \lim_{\varphi \rightarrow \infty} \frac{\varphi}{\omega} \ln \left[\frac{\varphi^{2+D^2}}{\varphi^{2+(D+T)^2}} \right]$$

Now

$$\ln \left[\frac{\varphi^{2+D^2}}{\varphi^{2+(D+T)^2}} \right] = \ln \left[1 - \frac{(D+T)^2 - D^2}{\varphi^{2+(D+T)^2}} \right]$$

which goes to zero as $1/\varphi^2$ when φ becomes large. Therefore the limit will go to zero as φ approaches infinity. The derivative in the second term of A gives

$$d \left(\ln \left[\frac{\varphi^{2+D^2}}{\varphi^{2+(D+T)^2}} \right] \right) = \frac{\varphi^{2+(D+T)^2}}{\varphi^{2+D^2}} d \left[\frac{\varphi^{2+D^2}}{\varphi^{2+(D+T)^2}} \right]$$

So that

$$d \left(\ln \left[\frac{\varphi^{2+D^2}}{\varphi^{2+(D+T)^2}} \right] \right) = 2\varphi \frac{(D+T)^2 - D^2}{(\varphi^{2+D^2}) \varphi^{2+(D+T)^2}} d\varphi$$

Upon substitution the integral becomes

$$A = -\frac{1}{\omega^2} \int_0^{\infty} 2\varphi (\sin \omega \varphi - \omega \varphi \cos \omega \varphi) \frac{(D+T)^2 - D^2}{(\varphi^{2+D^2}) \varphi^{2+(D+T)^2}} d\varphi$$

From the integration tables (Dewight, 1961)

$$\int_0^{\infty} \frac{X \sin mX dX}{(a^2+X^2)(b^2+X^2)} = \frac{\pi}{2} \left(\frac{e^{-mb} - e^{-ma}}{a^2 - b^2} \right)$$

and using Leibnitz' rule

$$\begin{aligned} \frac{\partial}{\partial m} \int_0^{\infty} \frac{X \sin mX dX}{(a^2+X^2)(b^2+X^2)} &= \frac{\pi}{2} \frac{\partial}{\partial m} \left(\frac{e^{-mb} - e^{-ma}}{a^2 - b^2} \right) \\ \int_0^{\infty} \frac{X^2 \cos mX dX}{(a^2+X^2)(b^2+X^2)} &= \frac{\pi}{2} \left(\frac{ae^{-ma} - be^{-mb}}{a^2 - b^2} \right) \end{aligned}$$

Which gives upon substitution

$$A = - \frac{\pi}{\omega} \left(\left[1+D \right] e^{-D\omega} - \left[1+(D+T) \right] e^{-(D+T)\omega} \right) \quad (2)$$

The next terms in Equation (1) are

$$B = 2 \int_0^{\infty} \tan^{-1} (D/\phi) \sin \omega \phi d\phi \quad (3)$$

and

$$C = 2 \int_0^{\infty} \tan^{-1} \left[(D+T)/\phi \right] \sin \omega \phi d\phi \quad (4)$$

These are of the form

$$I = 2 \int_0^{\infty} \tan^{-1} (a/X) \sin mX dX$$

The tables (Dewight, 1961) give for this integral

$$I = - \frac{\pi}{m} (1 - e^{-mX})$$

Upon substitution Equations (3) and (4) become

$$B = - \frac{\pi}{\omega} (1 - e^{-D})$$

$$C = - \frac{\pi}{\omega} \left[1 - e^{-(D+T)} \right]$$

Now

$$F_f(\omega) = \frac{2\gamma\sigma}{2\pi} \left[A + DB - (D+T)C \right] \quad (5)$$

Substituting A, B, and C into (5) and rationalizing yields

$$F_f(\omega) = \sqrt{2\pi} \gamma \sigma \left(\frac{1}{\omega^2} \left[e^{-(D+T)\omega} - e^{-D\omega} \right] - \frac{T}{\omega} \right) \quad (6)$$

APPENDIX C

Description of the Transform Program

Numerical integrations to find the Fourier Transforms of the gravitational anomalies were performed on the IBM 1620 computer located at Oregon State University. The numerical method employed was that of using the Newton-Cotes Quadrature Formulas of the closed type (Milne, 1949). These formulas are of the type

$$\int_{X_0}^{X_n} f(X) dX = \sum_{i=0}^n A_i f(X_i) \quad (1)$$

The coefficients, A_i , are obtained by the method of undetermined coefficients. The interval $h = |X_{i+1} - X_i|$ must be the same for each i .

In the case of the Fourier Transform Equation (1) becomes

$$F(\omega) = \int_{X_0}^{X_n} f(X) \begin{pmatrix} \cos \omega X \\ \sin \omega X \end{pmatrix} dX = \sum_{i=0}^n A_i f(X_i) \begin{pmatrix} \cos X_i \\ \sin X_i \end{pmatrix} \quad (2)$$

The computer program used in this research utilized Equation (2) with $n = 8$. Data points along the profile were stored in the computer's memory, and Equation (2) was applied to successive intervals along the profile. This was done for different frequencies until the numerical representation of the transform was obtained.

The maximum error inherent in this method is given by

$$E = \frac{2368 y^{(10)} h^{11}}{467775} \quad (3)$$

where $y^{(10)}$ is the maximum value of the tenth derivative of $f(X)$.

This maximum value is in the interval of integration. However, there are two other errors which are associated with the above method of finding the Transform (Hurwitz and Zweifel, 1956). These are:

(1) The Fourier Transform is an integral over an infinite interval, and the numerical integration must be terminated at some finite value. Thus, there is some "cut off" error. In this research the integration was terminated when the anomaly was 1/100 of its maximum amplitude. This error is larger at the lower frequencies. (2) The magnitude of the term added to the transform by integration over one cycle is the difference between the value for successive half cycles. This is illustrated in Figure 9. The value of the integral from $X = 0$ to

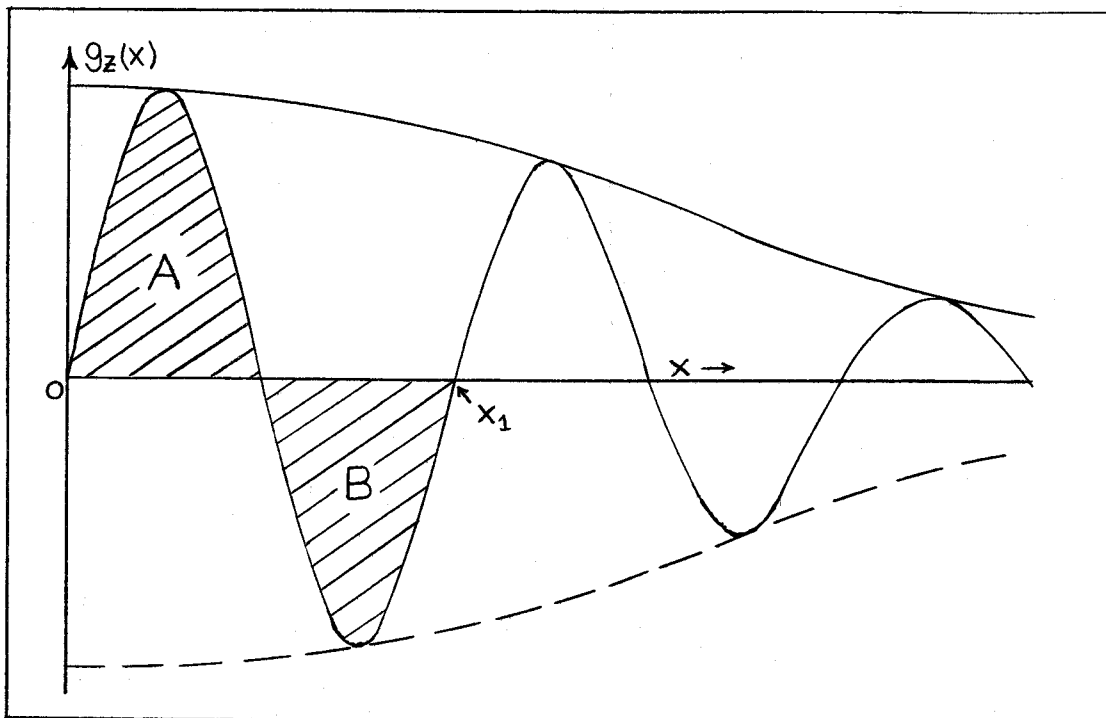


Figure 9. Magnification of error by subtraction of successive half cycles.

$X = X_1$ is the difference between the area A and the area B. At high frequencies the cosine or sine terms oscillate rapidly so that the difference between A and B may be much smaller than either A or B. When this happens the error given by Equation (3) will be magnified. In this research it was found that this type of error became appreciable when the value of the transform was less than 10^{-3} of its maximum value.